Available online at www.sciencedirect.com
SCIENCE DIRECT®
Biochimica et Biophysica Acta 1655 (2004) 149–157
BIOCHIMICA ET BIOPHYSICA ACTA
BBA
www.bba-direct.com

Review

The first spectroscopic model for the S_1 state multiline signal of the OEC

Wen-Yuan Hsieh[a], Kristy A. Campbell[b,1], Wolfgang Gregor[b], R. David Britt[b,*], Derek W. Yoder[a], James E. Penner-Hahn[a,c,*], Vincent L. Pecoraro[a,*]

[a] Department of Chemistry, University of Michigan, Ann Arbor, Michigan MI 48109-1055, USA
[b] Department of Chemistry, University of California, Davis, CA, USA
[c] Biophysics Research Division, University of Michigan, Ann Arbor, Michigan MI 48109-1055, USA

Received 11 June 2003; received in revised form 5 December 2003; accepted 5 December 2003

Abstract

The parallel-mode electron paramagnetic resonance (EPR) spectrum of the S_1 state of the oxygen-evolving complex (OEC) shows a multiline signal centered around $g=12$, indicating an integer spin system. The series of $[Mn_2(2\text{-}OHsalpn)_2]$ complexes were structurally characterized in four oxidation levels ($Mn^{II}{}_2$, $Mn^{II}Mn^{III}$, $Mn^{III}{}_2$, and $Mn^{III}Mn^{IV}$). By using bulk electrolysis, the $[Mn^{III}Mn^{IV}(2\text{-}OHsalpn)_2(OH)]$ is oxidized to a species that contains Mn^{IV} oxidation state as detected by X-ray absorption near edge spectroscopy (XANES) and that can be formulated as $Mn^{IV}{}_4$ tetramer. The parallel-mode EPR spectrum of this multinuclear $Mn^{IV}{}_4$ complex shows 18 well-resolved hyperfine lines center around $g=11$ with an average hyperfine splitting of 36 G. This EPR spectrum is very similar to that found in the S_1 state of the OEC. This is the first synthetic manganese model complex that shows an S_1-like multiline spectrum in parallel-mode EPR.

Keywords: S_1 state; Electron paramagnetic resonance (EPR); X-ray absorption near edge spectroscopy (XANES); Manganese complex

1. Introduction

Jerry Babcock was a pioneer in studies of the structure and function of the oxygen-evolving complex (OEC) of Photosystem II (PS II) [1,2]. Jerry's insight was often based on his interpretation of electron paramagnetic resonance (EPR) signals found for this enzyme, often as associated with relaxation of organic radicals by paramagnetic metal centers [3–6]. This relaxation occurs because the OEC utilizes a tetranuclear manganese cluster to catalyze the four-electron oxidation of water to molecular oxygen [7–9]. Four photon-induced charge separations at P_{680} generate four sequential oxidations of the OEC via tyrosyl radical (Y_z) intermediate. These oxidations give different oxidation states, known as S states, for the manganese cluster. The cyclic conversion of the S states is called the Kok cycle [10]. The S states are labeled S_0 through S_4, with S_0 the lowest oxidation state and S_4 the highest oxidation state.

EPR spectroscopy can provide information about the electronic structure of metal complexes. Comparison between the EPR spectra of model complexes [11] and those of the OEC has provided information about metal oxidation levels of the S states [12–14]. Different EPR multiline signals are seen for S_0 [15,16], S_1 [17,18], and S_2 [19] states. The S_2 state multiline signal was discovered in 1980 by Siderer and Dismukes [19]. More recently, in the presence of methanol, an S_0 state multiline signal was discovered [15,16]. Both multiline signals are centered around $g=2$ with perpendicular mode detection, and have more than 16 resolvable hyperfine lines. The g value and the number of hyperfine lines of the multiline signals have suggested that both S_0 and S_2 states are mixed-valence manganese cluster systems with $S=1/2$ ground states. The S_2 state signal is significantly narrower than the S_0 state signal; this is consistent with the S_2 state being more highly oxidized than the S_0 state. In contrast, the S_1 state is EPR silent using perpendicular-mode detection at 4 K and X-band frequencies. However, parallel-mode detected signals, which interrogate integer spin systems, have revealed a multiline signal centered around $g=12$ for the S_1 state [18].

* Corresponding authors. J.E. Penner-Hahn is to be contacted at the Department of Chemistry, University of Michigan, 930 North University Drive, Ann Arbor, MI 48109-1055, USA. V. L. Pecoraro, tel.: +1-734-763-1519; fax: +1-734-936-7628.
E-mail address: vlpec@umich.edu (V.L. Pecoraro).
[1] Current address: Micron Technology, Inc., 8000 S. Federal Way, Boise, ID 83707, USA.

0005-2728/$ - see front matter © 2004 Elsevier B.V. All rights reserved.
doi:10.1016/j.bbabio.2003.12.001

Since the discovery of the S_0 and S_2 state multiline signals, significant effort has been focused on preparing model complexes that can reproduce these signals and on simulating the observed EPR signals [11,20,21]. In contrast, there are no known model complexes that have an EPR signal similar to the S_1 state parallel-mode detected multiline signal. Herein, we present a tetranuclear Mn species, formulated as $[L_2Mn^{IV}Mn^{IV}(O)Mn^{IV}Mn^{IV}L_2]^{2+}$ (L=2OHsalpn), that exhibits an 18-line EPR signal centered around $g=11$ at 4 K and X-band frequency with parallel-mode detection. This 18-line signal is the first EPR signal to exhibit significant similarity to the S_0 state multiline signal both in line spacing and in overall spectral shape.

2. Reagents and materials

Salicylaldehyde was used as received from Aldrich without further purification. 1,3-Diamino-2-propanol was purchased from Fluka. Tetrabutylammonium hydroxide (1 M in methanol) was purchased from Aldrich and used without further purification. Reagent grade acetonitrile was purchased from Fisher and purified by stirring with anhydrous copper sulfate and distilled over phosphorus pentoxide. Reagent grade butylronitirle was purchased from Aldrich and treated with anhydrous copper sulfate and magnesium sulfate overnight. HPLC grade dichloromethane was purchased from Fisher and was distilled over calcium hydride.

2.1. Synthesis

2.1.1. Triethylamine hydrohexafluorophosphate ($N(Et)_3{\cdot}HPF_6$)

A solution of triethylamine (5 ml, 35.8 mmol) in 100 ml fresh distilled diethyl ether was prepared and degassed by bubbling a stream of N_2(g) through this solution. Concentrated hexafluorophosphoric acid (5 ml, 34.8 mmol) was added to the ether solution at 0 °C. During the addition, evolution of a white gas was observed. After 10 min of stirring, a white precipitate formed and was filtered under nitrogen. The isolated white solid was dried under vacuum overnight.

2.2. Synthesis of complexes $[Mn_2(2\text{-}OHsalpn)_2]^{0,+}$

The $H_3$2-OHsalpn ligand was prepared by the condensation of the 2 equivalents of the salicylaldehyde with 1 equivalent of 1,3-diaminopropan-2-ol in ethanol. The ligand can be isolated as crystalline solid.

2.2.1. $[Mn^{III}Mn^{III}(2\text{-}OHsalpn)_2]$

$H_3$2-OHsalpn (11.92 g, 40 mmol) was suspended in 250 ml methanol under vigorous stirring. Upon addition of sodium methoxide (27.5 ml, 120.2 mmol, 25 wt.% in methanol) the solid dissolved completely. $MnCl_2$ (5.03 g, 40 mmol) was added, resulting in a color change from golden yellow to dark brown. Air was bubbled through the reaction mixture overnight, which yielded a brown solid that was filtered and washed with cold methanol and ether. The brown solid was then redissolved in 400 ml of acetone without stirring. After 10 min, a black microcrystalline solid appeared. The solid was filtered and dried under vacuum. Yield: 10.1 g (72.1%), $[Mn^{III}Mn^{III}(2\text{-}OHsalpn)_2]{\cdot}$(acetone). Anal. found (calc): C: 58.56 (58.35); H: 4.78 (4.95); N: 7.39 (7.15).

2.2.2. $[Mn^{III}Mn^{IV}(2\text{-}OHsalpn)_2](PF_6)$

$[Mn^{III}Mn^{III}(2\text{-}OHsalpn)_2]$ (0.35 g, 0.5 mmol) was dissolved in 20 ml dichloromethane (CH_2Cl_2) and the solution was cooled to 0 °C in an ice-water bath. To this solution, 0.11 ml (0.55 mmol, 5 to 6 M in decane) *tert*-butyl hydroperoxide and 0.142 g (0.575 mmol) triethylammonium hexafluorophosphorate ($N(Et)_3{\cdot}HPF_6$) were added with stirring. Almost immediately after addition, the color of the solution turned from green brown to red brown and a brown precipitate formed. This solid was collected and washed with cold ether and dried under vacuum to give 0.31 g $[Mn^{III}Mn^{IV}(2\text{-}OHsalpn)_2](PF_6){\cdot}2.5H_2O$ (68% yield). Anal. found (calc): C: 45.82 (45.86); H: 3.73 (3.96); N: 5.96 (6.29).

2.2.3. $[Mn^{III}Mn^{IV}(2\text{-}OHsalpn)_2(OH)]$

$[Mn^{III}Mn^{IV}(2\text{-}OHsalpn)_2]$ (0.49 g, 0.7 mmol) was dissolved in 50 ml butylronitrile with gentle warming, and then the solution was cooled to 5 °C. Next, 0.154 ml (0.77 mmol) *tert*-butyl hydroperoxide was added under vigorous stirring and the solution color changed from dark green brown to dark red brown. After 2 min, the cold solution was added to 350 ml of cold diethyl ether to yield a cloudy brown solution. The solution was immediately filtered to give a brown powder, which was air-dried for 10 min and stored below −20 °C. Yield: 0.37 g (70%), $[Mn^{III}Mn^{IV}(2\text{-}OHsalpn)_2(OH)]{\cdot}2H_2O$. Anal. found (calc): C: 53.83 (54.18); H: 4.87 (4.65); N: 7.93 (7.44).

3. Instrumentation and physical methods

3.1. UV–Vis spectroscopy

UV–Visible spectra were recorded on a Perkin-Elmer Lambda 9 UV–Vis–NIR spectrometer equipped with a PE 3600 data station. Low-temperature (−60 °C) experiments were performed in a Dewar flask equipped with optical quality quartz windows and cooled with a dry ice/methanol bath. Low-temperature visible spectra were taken in acetone from 320 to 700 nm with a quartz flow-cell submerged into the Dewar flask. The sample solutions were injected into the quartz flow-cell. The temperature was monitored with a

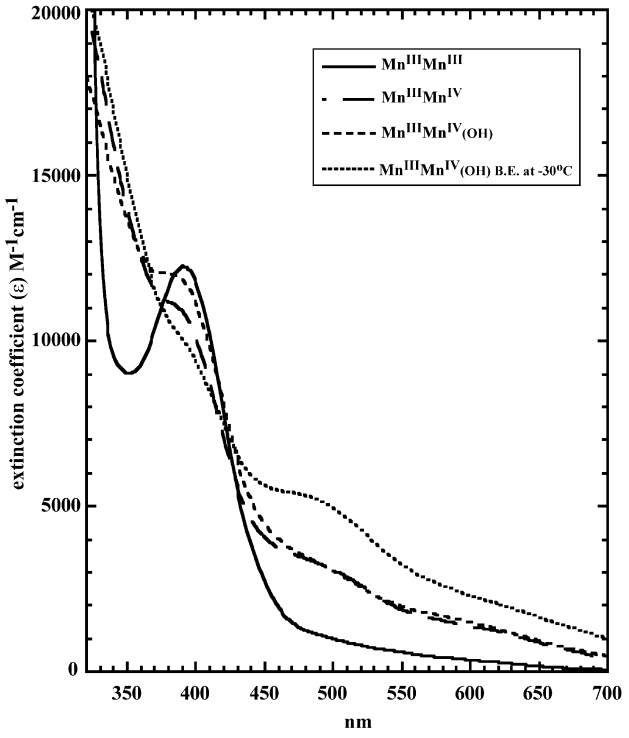

Fig. 1. The visible spectra of $[Mn(2\text{-}OHsalpn)]_2$ collected at -60 °C.

Type T thermocouple interfaced to a Barnant Thermocouple Thermometer.

The UV–Vis solution samples were prepared as follows: a 3 mM $[Mn^{III}Mn^{IV}(2\text{-}OHsalpn)_2](PF_6)$ solution (1.34 mg in 0.5 ml acetone), a 3 mM $[Mn^{III}Mn^{III}(2\text{-}OHsalpn)_2]$ solution (1.14 mg in 0.5 ml acetone), and a 3 mM $[Mn^{III}Mn^{IV}(2\text{-}OHsalpn)_2](OH)$ (1.13 mg in 0.5 ml acetone) solution were each diluted with 24 ml acetone at -78 °C to form 60 μM Mn solutions. The $Mn^{IV}Mn^{IV}$ sample was prepared by taking the 0.5 ml of bulk-electrolyzed 3 mM $[Mn^{III}Mn^{IV}(2\text{-}OHsalpn)_2](OH)$ solution and diluted with 24 ml acetone at -78 °C. The visible spectra were measured at -60 °C.

3.2. Electrochemistry

Cyclic voltammetry (CV) and bulk electrolysis studies were performed on a Bioanalytical System CV-27 electrochemical analyzer, scanning at 50 mV/s using glassy carbon as the working electrode, Pt wire as the auxiliary electrode, and Ag wire, Ag/AgCl, or $Ag/AgNO_3$ as the reference electrode. $TBAPF_6$ or $TBAClO_4$ (0.1 M) were used as the supporting electrolyte. Mn complexes were dissolved in acetonitrile and purged with N_2(g) before the CV was measured. Room temperature and low temperature (-30 °C) bulk electrolysis experiments were performed using Pt gauze as the working electrode, Pt wire as the auxiliary electrode, and Ag wire as the reference electrode in acetonitrile with 0.1 M $TBAPF_6$ as the supporting electrolyte.

CV and bulk electrolysis samples were prepared by dissolving Mn complexes in 0.1 M $TBAPF_6$ acetonitrile to make 3 mM Mn solutions. The low temperature (-30 °C) experiments were achieved by cooling the Mn solution in acetonitrile/dry ice bath. The temperature was monitored with a Type T thermocouple interfaced to a Barnant Thermocouple Thermometer. A cyclic voltammogram was measured with Ag/AgCl (room temperature) or $Ag/AgNO_3$ (-30 °C) as the reference electrode after the bulk electrolysis to check the redox potential of the complex.

3.3. EPR spectroscopy

The X-band continuous-wave (CW) perpendicular-mode EPR spectra were collected with a Brüker EMX200E spectrometer. Spectra were obtained in the range 4–60 K using an Oxford Instruments ESR-900 Continuous flow cryostat. Butylronitrile was used both as solvent and as glassing reagent for the reaction.

The X-band CW parallel-mode EPR spectra were collected on a Brüker ECS106 spectrometer. Cryogenic temperatures were obtained with an Oxford Instruments ESR-900 Continuous flow cryostat with an Oxford ITC503 temperature and gas flow controller. The EPR samples were prepared by taking aliquots of the bulk electrolyzed $Mn^{III}Mn^{IV}$ solutions and freezing them in liquid nitrogen.

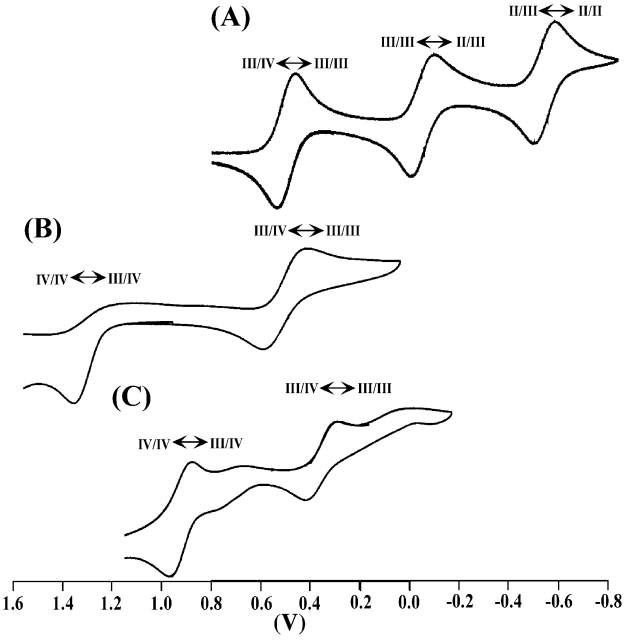

Fig. 2. CV of (A) $[Mn^{III}Mn^{IV}(2\text{-}OHsalpn)_2](ClO_4)$; (B) $[Mn^{III}Mn^{IV}(2\text{-}OHsalpn)_2](PF_6)$; (C) $[Mn^{III}Mn^{IV}(2\text{-}OHsalpn)_2](OH)$. A was measured at 20 °C on glassy carbon electrode against Ag/AgCl reference electrode and corrected to NHE potentials; B and C were measured at -10 °C on glassy carbon electrode against Ag wire reference electrode and corrected to NHE potentials. All CV were measured in acetonitrile.

3.4. X-ray absorption near edge structure (XANES)

X-ray absorption spectra were collected at the Stanford Synchrotron Radiation Laboratory (SSRL) beamline 7–3 using a Si(220) double-crystal monochromator. Harmonic rejection was achieved by detuning the incident intensity by 50%. Samples were kept at 10 K using an Oxford Instruments liquid He flow cryostat. Mn Kα fluorescence was detected using a Canberra 13-element solid state Ge detector. Energies were calibrated by reference to the distinct pre-edge feature of $KMnO_4$ (defined as 6543.3 eV) collected simultaneously with the data. Edge scans were typically defined with 5 eV spacing in the pre-edge region (6300–6500 eV, 1 s/point), 0.20 eV spacing in the edge region (6530–6570 eV, 3–4 s/point), and 2–10 eV spacing from 6570 to 6950 eV (2 s/point).

The XANES samples were prepared by injecting the bulk electrolyzed $Mn^{III}Mn^{IV}$ acetonitrile solutions into a 2-mm aluminum cell with Kapton tape windows at −78 °C. The samples were quickly frozen in liquid nitrogen and stored in liquid nitrogen until the experiments were completed.

Three or four scans were measured for each sample, and each scan was examined for glitches. The fluorescence from the good channels was averaged for each sample to give the raw data. The data were normalized, by scaling the data below and above the XANES region (20 eV below to 80 eV above the Mn K edge), to match tabulated X-ray absorption coefficients [22] by using MBACK [23]. The edge energy of each sample was determined by calculating of the first moment of the XANES spectrum [24]. The first moment is given in Eq. (1), where E is energy and $\mu(E)$ is the normalized X-ray cross-section.

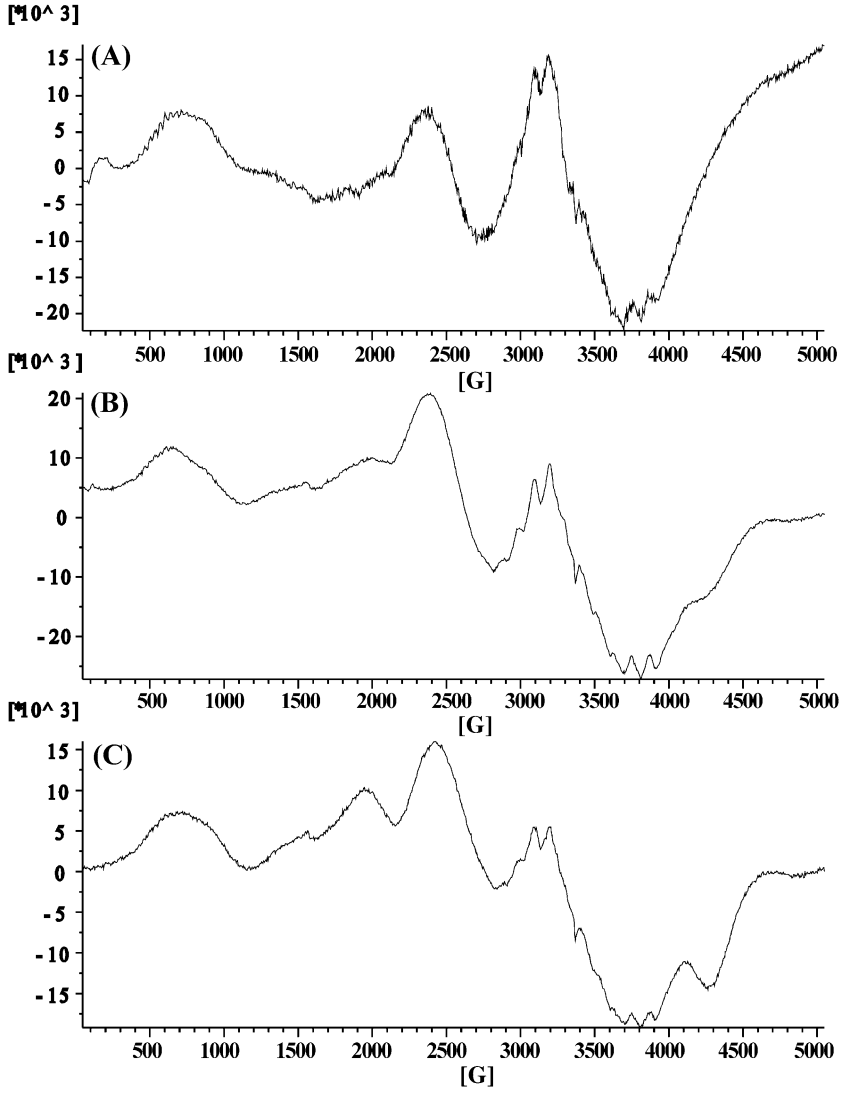

Fig. 3. Perpendicular-mode EPR spectra of bulk $[Mn^{IV}Mn^{IV}(2\text{-OHsalpn})_2(OH)]^+$ at (A) 4.2 K, (B) 10 K, and (C) 16 K. The Mn complex was dissolved in acetonitrile. The concentration of the Mn solution was 2 mM. EPR conditions: microwave frequency, 9.432 GHz; power, 20 mW; modulation amplitude, 10 G; modulation frequency, 100 kHz.

If $E \geq E_o$, $\mu(E) = aE^2 + bE + c$; otherwise $\mu(E) = 0$,

$$\text{Edge energy} < E > = \frac{\int_{Ei}^{Ef} E\mu(E)\mathrm{d}E}{\int_{Ei}^{Ef} \mu(E)\mathrm{d}E} = \frac{\left(\frac{a}{3}E^3 + \frac{b}{2}E^2 + cE\right)\Big|_{Eo}^{Ef}}{E_f - E_o} \quad (1)$$

4. Results

4.1. Electronic spectra of complexes

The visible spectra of the series of $[Mn_2(2\text{-OHsalpn})_2]$ complexes, collected from 320–700 nm at −60 °C in acetone, are shown in Fig. 1. The absorbance at 400 nm increases upon the addition of 1 equivalent of tetrabutylammonium hydroxide to $[Mn^{III}Mn^{IV}(2\text{-OHsalpn})_2]^+$. The extinction coefficient (ε) at 500 nm increases upon sequential oxidation of the Mn dimer.

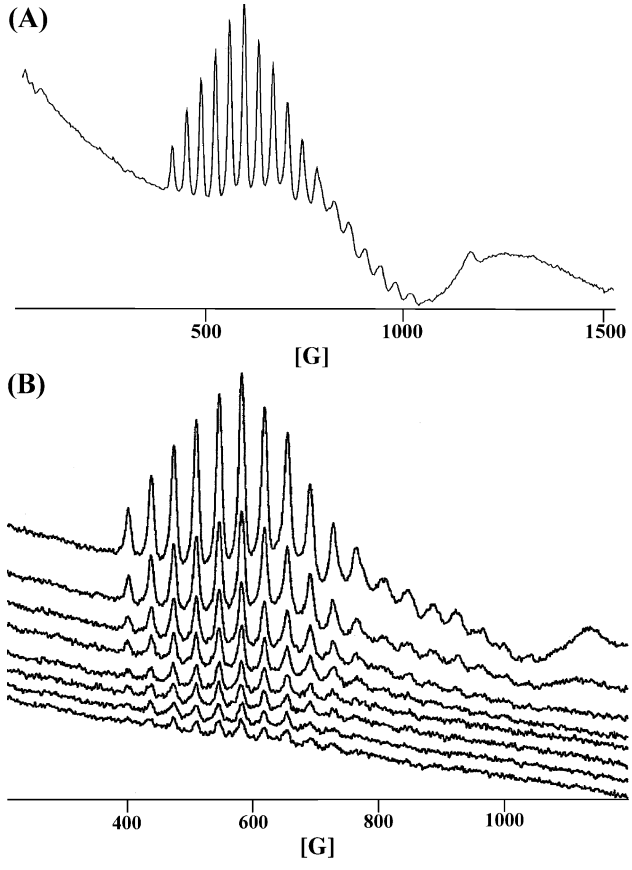

Fig. 4. Parallel-mode EPR spectra of $[Mn^{IV}Mn^{IV}(2\text{-OHsalpn})_2(OH)]^+$ at (A) 4 K; (B) temperature dependence, from 4 K (top) to 32 K (bottom) at 4 K increment. The Mn complex was dissolved in acetonitrile. EPR conditions: microwave frequency, 9.423 GHz; power, 20 mW; modulation amplitude, 8 G; modulation frequency, 100 kHz.

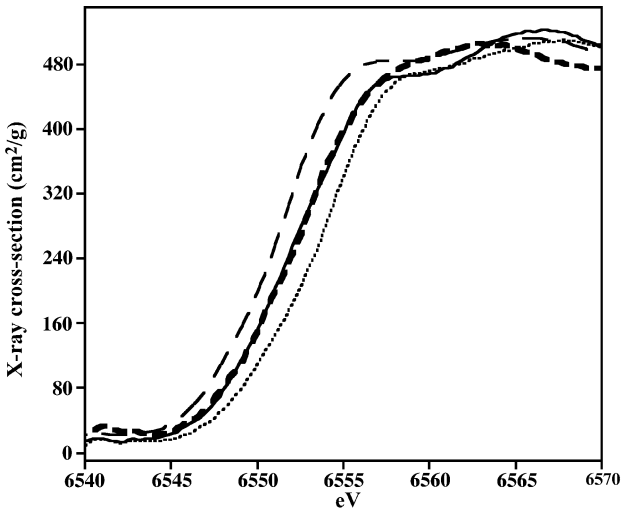

Fig. 5. XANES spectra of $Mn^{III}Mn^{III}$ (long dash), $Mn^{III}Mn^{IV}$ (solid line), bulk electrolyzed, $Mn^{III}Mn^{IV}$ (dotted), together with the S_1 state of the OEC (dash). Solid and dash lines overlap from 6545 to 6556 eV.

4.2. Electrochemistry

The cyclic voltammagram (CV) of $[Mn^{III}Mn^{IV}(2\text{-OHsalpn})_2](PF_6)$, shown in Fig. 2(A), indicates that reductions to $Mn^{III}{}_2$, $Mn^{II}Mn^{III}$, and $Mn^{II}{}_2$ are possible. All three transitions are reversible. In Fig. 2(B), the CV indicates that the oxidation of $Mn^{III}Mn^{IV}$ to $Mn^{IV}Mn^{IV}$ is also possible, but that this process is electrochemically irreversible. When 1 equivalent of tetrabutylammonium hydroxide (TBAOH) was added to $[Mn^{III}Mn^{IV}(2\text{-OHsalpn})_2](PF_6)$, the redox potential for the $Mn^{III}Mn^{IV} \rightleftharpoons Mn^{IV}Mn^{IV}$ and $Mn^{III}Mn^{III} \rightleftharpoons Mn^{III}Mn^{IV}$ couples shifted to lower potential, as shown in Fig. 2(C).

4.3. EPR spectra of the complexes

$[Mn^{III}Mn^{IV}(2\text{-OHsalpn})_2](PF_6)$, and $[Mn^{IV}Mn^{IV}(2\text{-OHsalpn})_2(OH)]^+$ are both EPR active with perpendicular mode detection. $[Mn^{III}Mn^{IV}(2\text{-OHsalpn})_2(OH)]$ is generated by the addition of 1 equivalent of tetrabutylammonium hydroxide (TBAOH) to $[Mn^{III}Mn^{IV}(2\text{-OHsalpn})_2](PF_6)$. $[Mn^{IV}Mn^{IV}(2\text{-OHsalpn})_2(OH)]^+$ can be prepared from $[Mn^{III}Mn^{IV}(2\text{-OHsalpn})_2(OH)]$ via single-electron bulk electrolysis. The variable-temperature, perpendicular-mode EPR spectrum of $[Mn^{III}Mn^{IV}(2\text{-OHsalpn})_2](PF_6)$ at 4 K in acetonitrile shows a 12-line signal centered at $g = 2$ [25]. The average peak-to-peak spacing (A) is about 105 G. When the temperature is increased, the 12-line signal broadens and a new broad signal grows at $g = 5.3$. Upon the addition of 1 equivalent of hydroxide ion to $[Mn^{III}Mn^{IV}(2\text{-OHsalpn})_2]^+$, the low-field signal shifts from $g = 5.3$ to $g = 4.5$, but the 12-line signal at 4 K is invariant [26].

The perpendicular-mode EPR spectrum of the $[Mn^{IV}Mn^{IV}(2\text{-OHsalpn})_2(OH)]^+$ in acetonitrile at 4 K shows three

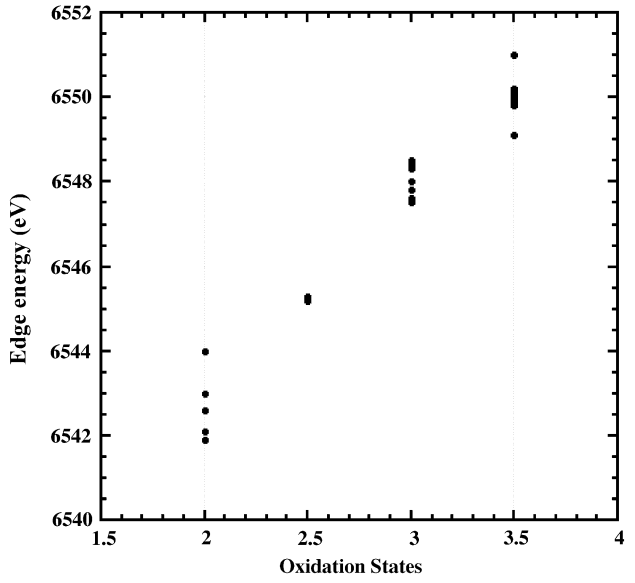

Fig. 6. Mn edge energy defined as the first moment of the XANES spectra (see text) different oxidation states. The data were collected SSRL as frozen solution.

broad signals at $g=9.2$, $g=2.8$, and $g=2$. There is also a weak multiline signal at $g=11$ with at least nine resolvable lines and a small signal at very low field (160 G). The multiline signal shows an average hyperfine splitting value (A) about 36 G. As the temperature increases, the intensity of the multiline signal decreases and two new broad signals grow at $g=3.45$ and $g=1.56$, as shown in Fig. 3. The $[Mn^{IV}Mn^{IV}(2\text{-OHsalpn})_2(OH)]^+$ is also EPR active in parallel mode (Fig. 4). The parallel-mode EPR spectrum show an 18-line signal centered at $g=11$ at 4 K with average A about 36 G. The intensity of the 18-line signal decreases as the temperature increases and the sample is EPR silent above 35 K, as shown in Fig. 4.

4.4. XANES spectral analysis

The XANES spectra for $[Mn^{III}Mn^{III}(2\text{-OHsalpn})_2]$, $[Mn^{III}Mn^{IV}(2\text{-OHsalpn})_2]^+$, and bulk electrolyzed $[Mn^{III}Mn^{IV}(2\text{-OHsalpn})_2]^+$ are compared in Fig. 5. The average Mn edge energy shifts by approximately 1.9 eV between each successive oxidation. For comparison, the XANES spectrum of the S_1 state of the OEC [27] is also included in Fig. 5. As noted previously, the XANES spectrum for the S_1 state has an energy most consistent with an average oxidation of 3.5. The edge energies can be quantitated using a first-moment calculation [24,28] as described above (Eq. (1)). The first moment for the series of $[Mn(2\text{-OH-X-salpn})]_2$ (X = H, 5-Cl, 3,5-Cl_2, 5-NO_2) complexes are compared in Fig. 6.

5. Discussion

The manganese center is responsible for the oxidation of two water molecules to liberate O_2, $4H^+$, and $4e^-$. Five distinct oxidation states of the enzyme, S_0–S_4, have been identified with S_0 being the most reduced state and S_4 being the most highly oxidized. The transitions from $S_0 \rightarrow S_1$ and $S_1 \rightarrow S_2$ are generally accepted to involve manganese-centered oxidation. The oxidation state of the S_2 state is mostly agreed to be $Mn^{III}Mn^{IV}{}_3$. With this formulation, the oxidation states of S_1 and S_0 states will be $Mn^{III}{}_2Mn^{IV}{}_2$ and either $Mn^{III}{}_3Mn^{IV}$ or $Mn^{II}Mn^{III}Mn^{IV}{}_2$, respectively. Both S_0 and S_2 states have an odd number for the sum of the manganese formal charge (S_0, 13; S_2, 15), while the S_1 state has an even number, 14. This latter point imposes that the S_1 state should be a non-Kramers system.

Zheng and Dismukes [29] have suggested an $Mn^{III}{}_3Mn^{IV}$ oxidation states for S_2 based on simulation of the S_2 multiline signal. In this alternative formulation, the oxidation state of S_1 would be $Mn^{III}{}_4$. Fig. 5 compares the XANES spectra for the S_1 state, $Mn^{III}Mn^{III}$, $Mn^{III}Mn^{IV}$, and bulk electrolyzed $Mn^{III}Mn^{IV}$. It is clear that the S_1 state and $Mn^{III}Mn^{IV}$ model overlap in the edge region, confirming the $Mn^{III}{}_2Mn^{IV}{}_2$ oxidation state assignment for S_1.

The redox potential of the $Mn^{III}Mn^{III} \rightleftharpoons Mn^{III}Mn^{IV}$ couple of $[Mn^{III}Mn^{IV}(2\text{-OHsalpn})_2]^+$ is 500 mV (vs. NHE). When 1 equivalent of hydroxide ion is added, the redox potential shifts to 250 mV (vs. NHE) reflecting the easier oxidation of $[Mn^{III}Mn^{IV}(2\text{-OHsalpn})_2(OH)]$. The hydroxide ion also affects the redox potential of the $Mn^{III}Mn^{IV} \rightleftharpoons Mn^{IV}Mn^{IV}$ couple, shifting the potential by about 500 mV toward more negative potentials. Lowering the redox potential of the $Mn^{III}Mn^{IV}(OH) \rightleftharpoons [Mn^{IV}Mn^{IV}(OH)]^+$couple makes the $[Mn^{IV}Mn^{IV}(2\text{-OHsalpn})_2(OH)]^+$ more accessible by bulk electrolysis. The added hydroxide anion can act as a ligand to the Mn, breaking a bridging alkoxide bond. This changes the $[Mn^{III}Mn^{IV}(2\text{-OHsalpn})_2]^+$ from a symmetric dimer to the asymmetric dimer $[Mn^{III}Mn^{IV}(2\text{-OHsalpn})_2(OH)]$. Hydroxide ion also balances the positive charge on the $Mn^{III}Mn^{IV}$ dimer, giving a neutral $Mn^{III}Mn^{IV}(OH)$ species. Single-electron bulk electrolysis oxidizes $Mn^{III}Mn^{IV}$ to $Mn^{IV}Mn^{IV}$.

Srinivasan et al. [30] have shown that when $[Mn^{III}(salen)]^+$is oxidized by either *meta*-chloroperbenzoic acid or iodosylbenzene, a new absorption band can be observed at 530 nm. The formation of this new visible band was attributed to the formation of $[Mn^{IV}(salen)(\mu\text{-}O)Mn^{IV}(salen)]^{2+}$ species. The visible spectra of the $[Mn^{III}Mn^{III}(2\text{-OHsalpn})_2]$, $[Mn^{III}Mn^{IV}(2\text{-OHsalpn})_2]^+$, $[Mn^{III}Mn^{IV}(2\text{-OHsalpn})_2(OH)]$, and bulk electrolyzed $[Mn^{III}Mn^{IV}(2\text{-OHsalpn})_2(OH)]$ all show an absorbance increase around 500 nm region upon the stepwise oxidation. The increased absorbance at 500 nm for bulk electrolyzed $[Mn^{III}Mn^{IV}(2\text{-OHsalpn})_2(OH)]$ supports the oxidation of $Mn^{III}Mn^{IV}$ to $Mn^{IV}Mn^{IV}$ and is also consistent with the findings of Srinivasan for the formation of $\{[Mn^{IV}(2\text{-OHsalpn})]_2O[Mn^{IV}(2\text{-OHsalpn})]_2\}^{2+}$species.

The Mn edge energies of the series of $[Mn(2\text{-OH-X-salpn})]_2$ complexes from $Mn^{II}Mn^{II}$ to $Mn^{III}Mn^{IV}$ were

measured previously using XANES spectroscopy [31]. As shown in Fig. 6, the edge energy increases by 5.3 ± 0.9 eV from $Mn^{II}Mn^{II}$ to $Mn^{III}Mn^{III}$, and from $Mn^{III}Mn^{III}$ to $Mn^{III}Mn^{IV}$ the edge energy increases by 2.0 ± 0.5 eV. The edge energy difference between $Mn^{III}Mn^{IV}$ and bulk electrolyzed $Mn^{III}Mn^{IV}$ is about 1.8 eV, which is consistent with oxidation by one electron per two Mn, to give the $Mn^{IV}Mn^{IV}$ oxidation state. In addition to the XANES spectra, EXAFS data (not shown) were also collected in an attempt to observe outer-shell scattering for the various Mn–Mn interactions. However, such scattering was not observed in the EXAFS spectra. This is not necessarily surprising, since the two Mn atoms in the $Mn^{IV}Mn^{IV}$ complex are bridged by only one alkoxo-bridge. On the other hand, EPR spectroscopy is sensitive to the weak coupling in such systems.

The perpendicular-mode EPR spectrum of the bulk electrolyzed $Mn^{III}Mn^{IV}$ species at 4 K shows a weak multiline signal at lower field and three broad features at higher field; these EPR signals show strong temperature dependence. The parallel-mode EPR spectrum of the same species at 4 K shows an 18-line signal, which decreases in intensity as the temperature increases. The EPR signal intensity follows a Curie Law ($1/T$) behavior as the temperature is changed, demonstrating that this multiline signal arises either from a ground state or from a very low-lying excited state. From the electrochemistry and XANES data described above, it is cleared that the 18-line parallel-mode EPR signal arises from an all Mn^{IV} species. A possible origin of this signal is an oxo-bridged tetranuclear Mn^{IV} cluster, $\{[Mn^{IV}(2\text{-OHsalpn})]_2O[Mn^{IV}(2\text{-OHsalpn})]_2\}^{2+}$, resulting from the dimerization of two $[Mn^{IV}Mn^{IV}(2\text{-OHsalpn})_2(OH)]^+$ molecules. This possibility arises directly from the large number of apparent hyperfine features in the parallel-mode spectrum. A $Mn^{IV}Mn^{IV}$ or $Mn^{III}Mn^{III}$ [13] dimer with equivalent or near equivalent Mn coordination environments is expected to show only 11 hyperfine lines. Therefore, the presence of more than 11 hyperfine lines is suggestive of a higher nuclearity Mn complex.

There could be other possible origins for the 18-line signal. One possibility is sample heterogeneity, where more than one species contribute to the signal. However, the 18-line spectrum, at least qualitatively, has a very clean appearance, with even line spacing across the signal and a smooth progression of intensities. The spectrum appears identical regardless of whether the sample was prepared by electrochemical oxidation, as described here, or by chemical oxidation with *meta*-chlorobenzoic acid [32], and samples with incomplete oxidation, showing different degree of $Mn^{III}Mn^{IV}$ background signals (multiline at $g=2$) in perpendicular mode. They all show the identical 18-line line shape in parallel mode (data not shown). If the 18-line signal arose from, for example, an 11-line dimeric species with a second species contributing seven to eight additional hyperfine lines, what would be the origin of the hyperfine structure presented by the second species, and how likely is it that the features would overlap so cleanly in both line spacing and intensity?

Another possibility for the multiline signal that has greater than 11 lines could arise from a dimer or even a monomer, because integer spin complexes can present multiple fine structure transitions. For example, a S = 2 $[Mn^{III}(salen)]^+$ complex presents more than six lines that is expected from ^{55}Mn hyperfine alone, though the line shape shifts to a clean six-line spectrum upon binding of *N*-methylmorpholine *N*-oxide (NMO) [33]. However, the line shape of the six-line signal from $[Mn^{III}(salen)]^+$ complex does not show the clean progression of intensities seen in the 18-line spectrum. More importantly, the line shape of the $[Mn^{III}(salen)]^+$ complex shifts with temperature, whereas the 18-line signal line shape appears invariant (within the finite S/N level) over 4–32 K temperature range, shown in Fig. 4. Temperature-dependent spectra occur naturally with multiple fine structure transitions as different spin manifolds become differentially populated as the temperature is varied.

We are working on getting good EPR simulations of the 18-line signal to address the issues described above. For example, can we find good simulation parameters with a tetranuclear model that gives a good match to the signal? A systematic variation of the parameters in rigorous tetramer simulation is very time consuming for this case because of the need for four ^{55}Mn hyperfine components, as well as the electron spin $S>1/2$, so large matrices must be diagonalized and a number of parameters varied, including the electron spin S. (See Ref. [13] for an example of an S_1 state simulation.) What values of S might be present in a linear tetranuclear Mn complex of the sort proposed? If the intermanganese couplings are all antiferromagnetic, then

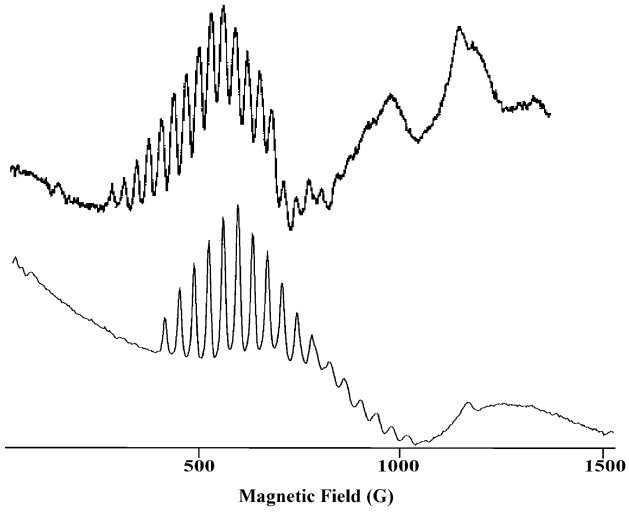

Fig. 7. Comparison of the parallel-mode EPR spectra of the S_1 state in OEC (top) and $[Mn^{IV}Mn^{IV}(2\text{-OHsalpn})_2(OH)]^+$(bottom). EPR conditions: temperature 4 K; microwave frequency, 9.432 GHz; power, 20 mW; modulation amplitude, 10 G; modulation frequency, 100 kHz.

the ground state will be $S=0$. If the couplings are weak, a low-level excited state may provide the origin for the signal. However, the signal intensity follows Curie law behavior to 4.2 K; this indicates that any low-level excited state must be very low in energy. Alternatively, there may be ferromagnetic couplings between Mn ions [34–36], in which case a high-spin ground state (up to $S=6$) could be produced.

The parallel-mode EPR spectrum of the S_1 state shows a multiline signal centered around $g=12$ at 4 K, with about 18–20 resolvable lines. The spectral width is about 800 G and the line spacing is about 32 G. The parallel-mode, 18-line signal found in the low field region ($g=11$) shows great similarity, in both g values and hyperfine structure, to that observed for the S_1 state parallel-mode EPR signal in the OEC (Fig. 7), although the spectral width of the 18-line signal (600 G) is somewhat less than the multiline signal (800 G) in the S_1 state of the OEC. The smaller spectral width is consistent with the S_1 state having a lower $Mn^{III}{}_2Mn^{IV}{}_2$ oxidation state relative to the all $Mn^{IV}{}_4$ in the $\{[Mn^{IV}(2\text{-OHsalpn})]_2O[Mn^{IV}(2\text{-OHsalpn})]_2\}^{2+}$ as shown in Fig. 5.

So far, there is no crystallographic data for the species that responsible for the 18-line signal. But it is our belief that the best molecular model for this species is two $[Mn^{IV}(2\text{-OHsalpn})]_2$ bridged by an single oxygen atom to form a $Mn^{IV}{}_4$ tetramer.

6. Conclusion

$\{[Mn^{IV}(2\text{-OHsalpn})]_2O[Mn^{IV}(2\text{-OHsalpn})]_2\}^{2+}$ was formed during the electrochemical oxidation of $[Mn^{III}Mn^{IV}(2\text{-OHsalpn})_2(OH)]$. The parallel-mode EPR spectrum of this species is very similar to the parallel-mode EPR spectrum of the S_1 state of the OEC. This is the first synthetic Mn complex species that exhibits a multiline signal reminiscent of the S_1 state signal of the OEC, suggesting that the Mn cluster remains as a tetramer in the S_1 state. It is noteworthy that neither EPR nor XANES alone was sufficient to define the nuclearity and oxidation state of the oxidizing cluster but that the two combined give a good description of the cluster core.

Acknowledgements

This research was supported in part by the National Institutes of Health (GM-39406 to VLP; GM-45205 to JEPH; and GM-48242 to RDB). DWY was supported in part by a Molecular Biophysics Training Grant from the NIH. XAS measurements were collected at SSRL, which are funded by the Department of Energy, Office of Basic Energy Sciences. The authors (WYH and DWY) thank Dr. Tsu-Chien Weng for useful discussion on determining XANES edge energy and providing normalization and first moment programs.

References

[1] G.T. Babcock, R.E. Blankenship, K. Sauer, Reaction-kinetics for positive charge accumulation on water side of chloroplast Photosystem II, FEBS Lett. 61 (1976) 286–289.
[2] G.T. Babcock, B.A. Barry, R.J. Debus, C.W. Hoganson, M. Atamian, L. McIntosh, I. Sithole, C.F. Yocum, Water oxidation in Photosystem II: from radical chemistry to multielectron chemistry, Biochemistry 28 (1989) 9557–9565.
[3] G.T. Babcock, in: P. Mathis (Ed.), Photosynthesis: From Light to Biosphere, vol. II, Kluwer Academic Publishing, Netherlands, 1995, pp. 209–215.
[4] C. Tommos, X.-S. Tang, K. Warncke, C.W. Hoganson, S. Styring, J. McCracken, B.A. Diner, G.T. Babcock, Spin-density distribution, conformation, and hydrogen bonding of the redox-active tyrosine Y_Z in Photosystem II from multiple electron magnetic-resonance spectroscopies: implications for photosynthetic oxygen evolution, J. Am. Chem. Soc. 117 (1995) 10325–10335.
[5] F. Dole, B.A. Diner, C.W. Hoganson, G.T. Babcock, R.D. Britt, Determination of the electron spin density on the phenolic oxygen of the tyrosyl radical of Photosystem II, J. Am. Chem. Soc. 119 (1997) 11540–11541.
[6] C. Goussias, A. Boussac, A.W. Rutherford, Photosystem II and photosynthetic oxidation of water: an overview, Philos. Trans. R. Soc. Lond., B 357 (2002) 1369–1381.
[7] B.A. Diner, F. Rappaport, Structure, dynamics, and energetics of the primary photochemistry of Photosystem II of oxygenic photosynthesis, Annu. Rev. Plant Biol. 53 (2002) 551–580.
[8] T.G. Carrell, A.M. Tyryshkin, G.C. Dismukes, An evaluation of structural models for the photosynthetic water-oxidizing complex derived from spectroscopic and X-ray diffraction signatures, J. Biol. Inorg. Chem. 7 (2002) 2–22.
[9] B. Kok, B. Forbush, M. McGloid, Cooperation of charges in photosynthetic O_2 evolution—1. A linear four step mechanism, Photochem. Photobiol. 11 (1970) 457–475.
[10] M. Zheng, S.V. Khangulov, G.C. Dismukes, V.V. Barynin, Electronic structure of dimanganese(II,III) and dimanganese(III,IV) complexes and dimanganese catalase enzyme: a general EPR spectral simulation approach, Inorg. Chem. 33 (1994) 382–387.
[11] J.M. Peloquin, R.D. Britt, EPR/ENDOR characterization of the physical and electronic structure of the OEC Mn cluster, Biochim. Biophys. Acta 1503 (2001) 96–111.
[12] R.D. Britt, J.M. Peloquin, K.A. Campbell, Pulsed and parallel-polarization EPR characterization of the Photosystem II oxygen-evolving complex, Annu. Rev. Biophys. Biomol. Struct. 29 (2000) 463–495.
[13] H. Mino, A. Kawamori, EPR studies of the water oxidizing complex in the S_1 and the higher S states: the manganese cluster and Y_z radical, Biochim. Biophys. Acta 1503 (2001) 123–137.
[14] J. Messinger, J.H. Robblee, W.O. Yu, K. Sauer, V.K. Yachandra, M.P. Klein, The S_0 state of the oxygen evolving complex in Photosystem II is paramagnetic: detection of EPR multiline signal, J. Am. Chem. Soc. 119 (1997) 11349–11350.
[15] K.A. Åhrling, S. Peterson, S. Styring, An oscillating manganese electron paramagnetic resonance signal from the S_0 state of the oxygen evolving complex in Photosystem II, Biochemistry 36 (1997) 13148–13152.
[16] S.L. Dexheimer, M.P. Klein, Detection of a paramagnetic intermediate in the S_1 state of the photosynthetic oxygen-evolving complex, J. Am. Chem. Soc. 114 (1992) 2821–2826.
[17] K.A. Campbell, J.M. Peloquin, D.P. Pham, R.J. Debus, R.D. Britt, Parallel polarization EPR detection of an S_1-state "Multiline" EPR signal in Photosystem II particles from *Synechocystis* sp. PCC 6803, J. Am. Chem. Soc. 120 (1998) 447–448.
[18] G.C. Dismukes, Y. Siderer, EPR spectroscopic observations of a manganese center associated with water oxidation in spinach chloroplasts, FEBS Lett. 121 (1980) 78–80.

[19] K. Hasegawa, M. Kusunoki, Y. Inoue, T.A. Ono, Simulation of S_2-state multiline EPR signal in oriented Photosystem II membranes: structural implications for the manganese cluster in an oxygen-evolving complex, Biochemistry 37 (1998) 9457–9465.
[20] V.L. Pecoraro, W.-Y. Hsieh, in: A. Sigel, H. Sigel (Eds.), Metal Ions in Biological Systems, vol. 37, Marcel Dekker, New York, 2000, pp. 429–504.
[21] W.H. McMaster, N.K. Del Grande, J.H. Mallett, J.H. Hubbel, Compilation of X-ray Cross Sections, vol. UCRL-50174, National Technical Information Services, Springfield, 1969.
[22] T.-C. Weng, G.S. Waldo, J.E. Penner-Hahn, manuscript in preparation.
[23] P.M. De Marois, Structure and Reactivity of Manganese in Photosystem II, University of Michigan, Ann Arbor, MI, 1999.
[24] T.-C. Weng, unpublished results.
[25] E.J. Larson, V.L. Pecoraro, in: V.L. Pecoraro (Ed.), Manganese Redox Enzymes, VCH Publishers, New York, 1992, pp. 1–28.
[26] M.T. Caudle, P. Riggs-Gelasco, A.K. Gelasco, J.E. Penner-Hahn, V.L. Pecoraro, Mechanism for the homolytic cleavage of alkyl hydroperoxides by the manganese(III) dimer $Mn^{III}{}_2(2\text{-OHsalpn})_2$, Inorg. Chem. 35 (1996) 3577–3584.
[27] E.Y. Yu, Structural Characterization of the Manganese Cluster in the Oxygen-Evolving Complex of Photosystem II Using Electron Paramagnetic Resonance, X-ray Absorption and X-ray Standing Wave Measurements, University of Michigan, Ann Arbor, MI, 1999.
[28] D.W. Yoder, Physical Characterization of Manganese Catalase and its Halide Bound Forms, University of Michigan, Ann Arbor, MI, 2003.
[29] M. Zheng, G.C. Dismukes, Orbital configuration of the valence electrons, ligand field symmetry, and manganese oxidation states of the photosynthetic water oxidizing complex: analysis of the S_2 state multiline EPR signal, Inorg. Chem. 35 (1996) 3307–3319.
[30] K. Srinivasan, P. Michaud, J.K. Kochi, Epoxidation of olefins with cationic (salen)Mn^{III} complexes. The modulation of catalytic activity by substituents, J. Am. Chem. Soc. 108 (1986) 2309–2320.
[31] P. Riggs-Gelasco, Structural Characterization of the Manganese Cluster of the Oxygen Evolving Complex of Photosystem II Using X-ray Absorption Spectroscopy, University of Michigan, Ann Arbor, MI, 1994.
[32] W.-Y. Hsieh, B.T. Farrer, B. Schmidt, T.-C. Weng, J.E. Penner-Hahn, K.A. Campbell, R.D. Britt, V.L. Pecoraro, Oxidation of $[Mn_2^{III/IV}(2\text{-OHSalpn})_2]^+$ using *meta*-chloroperbenzoic acid, manuscript in preparation.
[33] K.A. Campbell, M.R. Lashley, J.K. Wyatt, M.H. Nantz, R.D. Britt, Dual-mode EPR study of Mn(III) salen and the Mn(III) salen-catalyzed epoxidation of *cis*-beta-methylstyrene, J. Am. Chem. Soc. 123 (2001) 5710–5719.
[34] A. Geisselmann, P. Klufers, B. Pilawa, Binuclear homoleptic manganese(III,III) and manganese(IV,III) complexes with deprotonated D-mannose from aqueous solution, Angew. Chem., Int. Ed. Engl. 37 (1998) 1119–1121.
[35] C. Duboc-Toia, H. Hummel, E. Bill, A.-L. Barra, G. Chouteau, K. Wieghardt, Integer-spin multifrequency EPR spectroscopy of a ferromagnetically coupled, Oxo-bridged MnIVMnIV model complex, Angew. Chem., Int. Ed. Engl. 39 (2000) 2888–2890.
[36] T.M. Rajendiran, M.L. Kirk, I.A. Setyawati, M.T. Caudle, J.W. Kampf, V.L. Pecoraro, Isolation of the first ferromagnetically coupled Mn(III/IV) complex, Chem. Commun. (2003) 824–825.